# 1 "Pressure-driven microbial and viral dynamics on

# 2 individual sinking particles: implications for

# з carbon cycling"

- 4 Chloé M.J. Baumas<sup>\$, 1,2</sup>, Danny Ionescu<sup>\$, 3</sup>, Marc Garel<sup>1</sup>, Hans-Peter Grossart<sup>4,5</sup>, Christian
- 5 Tamburini<sup>#, 1</sup>, Mina Bizic<sup>#, 3</sup>
- 6 <sup>1</sup>Aix Marseille Univ, Université de Toulon, CNRS, IRD, MIO, Marseille, France
- <sup>2</sup>Department of Earth System Science, Stanford University, CA United States
- 8 <sup>3</sup>Department of Environmental Microbiomics, Technische Universität Berlin, Berlin, Germany
- 9 <sup>4</sup> Department of Plankton and Microbial Ecology, Leibniz Institute of Freshwater Ecology and
- 10 Inland Fisheries (IGB), Stechlin, Germany
- <sup>5</sup> Institute of Biochemistry and Biology, Potsdam University, Potsdam, Germany
- 12 §Authors contributed equally to this work
- <sup>#</sup>Corresponding authors: Christian Tamburini (christian.tamburini@mio.osupytheas.fr) and Mina
- 14 Bizic (<u>mina.bizic@tu-berlin.de</u>)

17 Statement

15

16

20

21

22

23

24

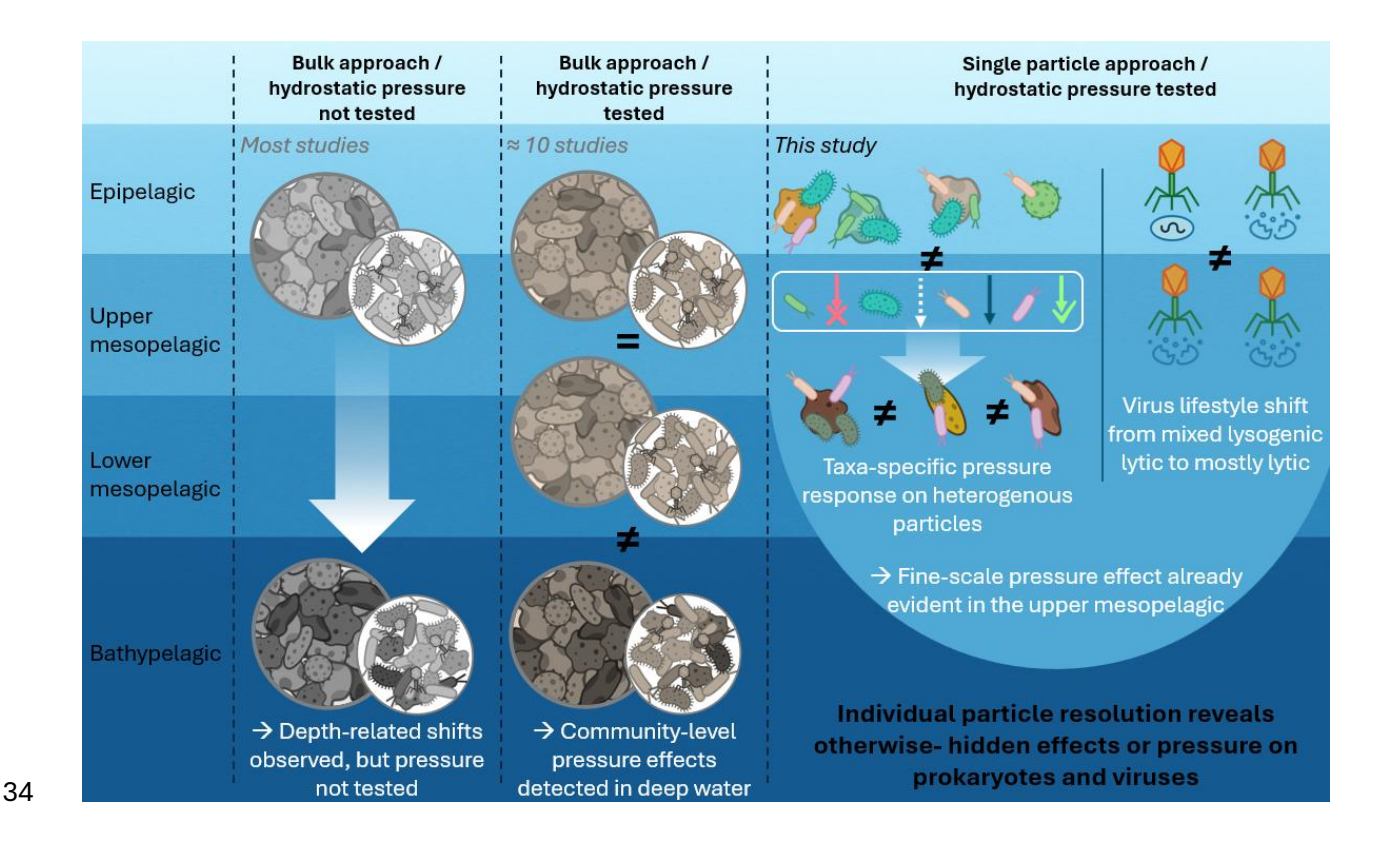
25

26

27

- 18 This manuscript is a non-peer-reviewed preprint submitted to EarthArXiv. It has not yet been peer-
- 19 reviewed or formally accepted for publication.

# Graphical abstract



Graphical abstract text: Contrary to previous study, we evaluated pressure effects in a controlled experiment, focusing on individual particles and microbial taxa. This revealed pressure effects occur at a much shallower depth and very heterogenously, differently than previously considered based on bulk analyzes. While some taxa don't make it to the mesopelagic, the effect on others ranges from positive through neutral to negative. We use our findings to discuss the potential implication for carbon sequestration in the ocean.

**Abstract** 

- The ocean's biological carbon pump (BCP) regulates atmospheric CO<sub>2</sub> by exporting organic
- 44 carbon from the surface to the deep. This process mainly depends on microbial communities

associated with sinking particles transforming organic matter. While many factors impact the BCP, we focus on the relationships between microbial communities, heterogenous particles and increasing hydrostatic pressure. We accessed metagenomic and transcriptomic data at the level of individual particles exposed to pressure mimicking gravitational sinking. We underscore the high variability among particles in terms of community composition and metabolic activity. Individualparticle analyses revealed significant heterogeneity, even within similar origin pointing to stochastic colonization. These challenge traditional assumptions of similar responses by different microorganisms, revealing intricate and variable processes that govern organic matter cycling. Under increased hydrostatic pressure, microbial diversity declined, with species-specific responses dominating on individual particles. We recognized piezosensitive microbes experiencing broad transcriptional declines, and piezotolerant showing resilience and/or enhanced overall transcriptional activity. Metabolic pathways essential for carbon cycling were altered and viral dynamics shifted notably with lytic viral forms becoming dominant, potentially increasing microbial mortality and altering nutrient cycling. Overall, our findings imply that accounting for particle heterogeneity and hydrostatic pressure allow to refine carbon flux models and predictions under changing ocean.

- 61 Keywords: Biological carbon pump, hydrostatic pressure, metabolic activities, respiration,
- 62 biodegradation, attached prokaryotes and virus, marine snow

### 1. Introduction

45

46

47

48

49

50

51

52

53

54

55

56

57

58

59

60

63

64

65

66

67

68

69

70

71

72

73

Oceanic photosynthesis converts 50-60 Gt C yr<sup>-1</sup> (one-quarter of anthropogenic CO<sub>2</sub> emissions) into biomass (Parekh et al. 2006; Passow and Weber 2025). Carbon trapped in organic particles (e.g. fecal pellets, zooplankton carcasses, phytoplankton cells, or other detritus) can rapidly sink through the water column exporting large quantities of atmospheric carbon through a process known as the biological carbon pump (BCP). Once exported below 1000 m depth, the carbon is thought to be sequestered for millennia (Siegel et al. 2023). Thus, atmospheric CO<sub>2</sub> concentration is closely linked to the BCP and its efficiency (Kwon et al. 2009). This has been the case for millions of years, and it is essential to predict how the BCP will respond to accelerated climate and anthropogenic impacts and their related biochemical changes (García-Martín et al. 2014; Martin et al. 2020). Below the photic zone (~200 m), heterotrophic organisms rely on sinking

particles as a primary carbon and nitrogen source, making the BCP critical for deep-sea ecosystems (including commercial fishing stocks) (Martin et al. 2020). Yet, measured biological carbon demand in the mesopelagic zone (~200–1000 m) frequently exceeds particle-derived supply, even when considering only prokaryotes (Burd et al. 2010; Baumas et al. 2023a). This mismatch underscores the complexity of the BCP despite its ecological and societal relevance.

Marine prokaryotes can be distinguished into free-living and particle-attached which points to their differences in lifestyle and ecology (Grossart 2010; Villalba et al. 2022). Whereas free-living prokaryotes depend on ambient dissolved organic carbon (DOC), those attached to particles solubilize particulate organic carbon (POC) via intense extracellular enzymatic activities to access C and nutrients from the particles they are colonizing on (Smith et al. 1992). Prokaryotes attached to sinking particles experience rapid environmental changes during particle descent (e.g. increasing hydrostatic pressure, decreasing in temperature and in POC quality). For instance, particles sinking at 150-500 m per day experience an increase in pressure of 1.5-5.0 MPa per day. We thus hypothesize that particle-attached communities leaving the euphotic zone are largely composed of piezotolerant or piezosensitive prokaryotes, which must withstand short-term fluctuations in pressure during descent, rather than the constant pressure conditions that characterize free-living prokaryotes.

Hydrostatic pressure is known to affect growth (e.g. Zobell and Johnson 1949; Zobell and Oppenheimer 1950), DNA synthesis (e.g., Bartlett et al. 2007), cell division (e.g., Bartlett 2002), membrane fluidity (e.g., DeLong and Yayanos 1985), storage lipids (Grossi et al. 2010), motility (e.g., Mullane et al. 2023), protein synthesis (Grossart and Gust 2009), enzymatic activity (e.g. Allen et al. 1999; Kish et al. 2012), and community composition (e.g. Grossart and Gust 2009). However, most of these studies were conducted on pure cultures and, thus, we cannot relate these settings to *in-situ* microbial activities and consequently BCP efficiency. Tracking the microbial degradation processes occurring during gravitational particle sinking *in-situ*, accounting for hydrostatic pressure changes, is difficult. Only a few systems exist to mimic the natural pressure variations during particle descent (e.g. de Jesus Mendes et al. 2007; Grossart and Gust 2009; Tamburini et al. 2009; Mendes and Thomsen 2012; Dong et al. 2018; Stief et al. 2021; Liu et al. 2022). Results from these systems show that hydrostatic pressure affects activities and also diversity of surface-originating prokaryotes. For instance, the increase in pressure can lead to a

significant inhibition of respiration (Stief et al. 2021; Tamburini et al. 2021) and protein production 104 105 (Grossart and Gust 2009), changes in enzymatic activities (Tamburini et al. 2006), organic matter 106 degradation (Tamburini et al. 2009), and inorganic matter dissolution (Tamburini et al. 2006, 2021; Riou et al. 2018), all of which result in drastic changes in diversity (Riou et al. 2018; Tamburini 107 et al. 2021; Stief et al. 2023). Though each study has focused on different microbial mechanisms, 108 they have all treated particles as bulk samples (except Stief et al. 2023). However it has been shown 109 110 that individual particles – even of the same source - are highly heterogenous and that averaging multiple particles generates an incorrect picture of composition and dynamics of the particle-111 attached microbiome (Bizic-Ionescu et al. 2018; Zäncker et al. 2019; Baumas et al. 2023b; Stief et 112 al. 2023; Baumas and Bizic 2024). 113 So far it is not technically possible to study the effect of pressure on *in situ* particles directly. The 114 only option to study pressure effects in situ was to compare the bulk of particles collected at 115 116 different depths. We therefore conducted pressure experiments using the particle sinking simulator 117 system (PASS, Tamburini et al., 2009), which allows mimicking, as closely as possible, environmental variations, e.g. pressure and temperature changes, during gravitational sinking of 118 119 particles in the ocean, controlling particles' history. In addition, this set up allowed us to analyse the samples at the individual particle level to understand the variability in microbial diversity and 120 121 metabolic activity at the individual particle's resolution. To analyze community composition and potential functional changes during particle sinking, we developed a new protocol enabling to 122 123 assess both metagenomic and metatranscriptomics data on the same individual particle for prokaryotes whose genome we could assemble. Those data were then coupled to biogeochemical 124 125 data (specifically POC and PON concentrations). We re-estimate microbial activities in terms of

### 2. Material & methods

#### 2.1 Particle origin

hydrostatic pressure.

126

127

128

129

Particles in this experiment were made of axenic cultures of *Thalassiosira guillardi* maintained at 14 °C, 12:12-h light-dark cycle (120 µmol photons m<sup>-2</sup> s<sup>-1</sup> irradiance), in F/2 medium enriched with vitamins (Guillard 1975; Guillard and Hargraves 1993). Cultures were then harvested (300

carbon utilization accounting for the heterogeneity among single particles and the increase of

mL) at the late exponential phase and transferred to a 2 L cylindric polycarbonate Nalgene® bottle prefilled with seawater. Seawater for the experiment was collected at 200 m during the PARTY cruise (May 2021, Mediterranean Sea, 42°47. 525°N 0.5°59. 814 E), pre-filtered through GFF filters (ref. 513-5244 Whatman®, VWR, US) to remove all living zooplankton and natural particles and stored in the dark at 4 °C. The full, bubble-free, bottle was placed on a roller table in complete darkness for 7 days to allow for formation of particles and their colonization by microorganisms from the surrounding seawater.

#### 2.2 SINking Particles Simulation Experiments (SINPAS Experiments)

#### 2.2.1 Particles preparation

140

141

142

143

144

145

146

147

148

149

Individual particles were transferred twice into Petri dishes containing fresh, sterile seawater to minimize the transfer of free-living microorganisms. After this washing step, particles were split equally into 20 aliquots using a McLane<sup>®</sup> splitter (ref. WSD-10). Two aliquots were used to evaluate individual particles for i) fluorescent microscopy (x1000) to study microbial colonization using DAPI (4',6-diamidino-2-phénylindole); and ii) for measuring sinking velocities of particles in a glass cylinder. The measured average sinking speed (43 m d<sup>-1</sup>) was used for our sinking experiments.

#### 2.2.2 Pressure experiments

All pressure experiments were conducted in June–July 2021 as depicted in Figure S1. Three pre-150 151 combusted 500 mL glass-bottles and six high-pressure bottles (HPBs, final volume 500 mL) were filled with sterile seawater (filtered and boiled). The HPBs were intensively washed with MilliQ 152 153 water and autoclaved prior to each experiment. Non-metal parts of the HPBs (piston, O-rings) were 154 bathed in 5% HCL (fin. conc.) and rinsed twice with MilliQ water. Two equal aliquots of particles from the McLane splitter were transferred into each bottle. Filling the bottles first with water 155 avoids breakage of particles when carefully transferred to the bottles with a wide-mouth pipette. 156 The three glass bottles, corresponding to initial (T0) triplicates, were immediately sub-sampled for 157 various parameters (see below). The six HPBs were immediately fitted onto the particle sinking 158 simulator (PASS) system (Tamburini et al. 2009). Three HPBs were kept at constant atmospheric 159 pressure (ATM) and three HPBs were continuously pressurized at a rate of 0.43 MPa d<sup>-1</sup> (HP) 160 corresponding to the measured sinking rate (~43 m d<sup>-1</sup>). Particles were kept in suspension by half-161

revolutions every minute of the 2-paired HPBs in temperature-regulated water baths. Both ATM and HP incubations were performed at a constant temperature of 13 ° C, agreeing with the *in-situ* temperature profile recorded during the PARTY cruise. The experiment was stopped when dissolved O<sub>2</sub> concentration reached 50 % of the initial concentration to avoid any anaerobic conditions (dissolved O<sub>2</sub> concentration method is described in supp data). The experiments were run for 12 days to reach a simulated depth of 516 m (corresponding to an increase of hydrostatic pressure from 0.1Mpa to 5.2 Mpa). At the end of the incubations, gentle depressurization was applied on the three HPBs under pressure. All six HPBs were then opened and transferred into precombusted glass bottles prior to sub-sampling. For OMICS analyses, individual particles were promptly. collected by carefully transferring them one by one with a wide-mouth pipette into cryotubes pre-filled with handmade RNAfixative solution (40 mL 0.5 M ethylenediamine tetraacetic acid (EDTA) [ref. EU0084, Euromedex], 25 mL 1 M sodium citrate (ref. S-4641, Sigma-Aldrich) and 700 g ammonium sulfate (ref. 21333.365 AnalaR NORMAPUR®, VWR) in 935 mL MQ water, pH adjusted to 5.2 using 1 M H2SO4). Samples were then placed at -80°C until analysis. Samples for POC/PON and DOC were collected and analyzed as detailed below.

### 2.3 OMICS analyses

162

163

164

165

166

167

168

169

170

171

172

173

174

175

176

177

178

#### 2.3.1 Extraction, amplification of individual particles

- 179 Individual particles were transferred from cryotubes into 1.5 mL RNAse and DNAse free
- 180 SafeLock Eppendorf® tubes. 1 µL of RiboLock RNAse Inhibitor (ref. EO0381, Thermo Fisher
- Scientific, US) and phosphate buffered saline (ref. 150343, Qiagen, Germany) were added to a
- 182 final volume of 4 µL. Cell lysis was then performed by four cycles of freeze/thaw, each 1 min in
- 183 liquid N<sub>2</sub> and 1 min at 65 °C. A denaturation step was then performed by adding 3 μL of D2 buffer
- from the REPLI-g single cell kit (ref. 150343, Qiagen, Germany) and incubation for 20 min at 65
- °C, followed by 3 μL of STOP solution according to the manufacturer's instruction.
- The High-Capacity cDNA Reverse Transcription Kit (Cat. 4368814, Thermo Fisher Scientific)
- 187 was used to generate cDNA from the RNA component of the mixed nucleic acids extracted. The
- final 20 µl reaction consisted of the 11 µl template extract with 2 µl reaction buffer, 0.75 µl dNTPs
- mix, 2 µl random heptamers, 1 µl reverse transcriptase, and 3.25 µl H<sub>2</sub>O. The reaction was done
- according to the manufacturer's instructions for 10 min at 25 °C, 120 min at 37 °C, and 5 min at
- 191 85 °C, after which the reaction was shortly cooled down to 4 °C and immediately used for whole

- 192 genome amplification (WGA). For WGA, 29 µl of REPLI-G single-cell reaction buffer (ref.
- A39391), and 2 μl of enzyme equiφ29 DNA polymerase (ref. A39391, 10 U/ul, Thermo Scientific)
- were added to each tube, followed by a 16 h incubation at 30°C, and 10 min inactivation at 65°C.
- The amplified DNA was quantified using a Quantus Fluorometer (Cat. E6150, Promega, Germany)
- and the QuantiFluor® ONE dsDNA System kit (Cat. E4870, Promega, Germany), after which they
- 197 were frozen at -20 °C till they were shipped for sequencing.

#### Sequencing

198

- 199 Shotgun sequencing was conducted using a NovaSeq 6000 sequencer using the S4 chip (2x150;
- 200 Illumina Inc San Diego, CA, USA) after shotgun Library Prep at the Rush University Genomics
- and Microbiome Core Facility. Genomic DNA samples were prepared for sequencing by an initial
- quantification using a Qubit 4 Fluorometer (Life Technologies, #Q32851, Grand Island, NY,
- 203 USA). Library preparation was performed using the Illumina DNA Prep Workflow with UDI
- 204 indexing (#20018705, 20027213 Illumina Inc. San Diego, CA, USA) according to the
- 205 manufacturer's instructions with 50 ng template input and 5 cycles of PCR. An equal-volume pool
- of all libraries was then made. The pool was quantified using a Qubit DNA High Sensitivity kit
- 207 (Life Technologies, #Q32851, Grand Island, NY, USA), and size distribution was assessed using
- an Agilent 4200 TapeStation System (Agilent Technologies, G2991AA, Santa Clara, CA, USA)
- with a TapeStation D5000 ScreenTape, ladder and assay (Agilent Technologies, # 5067-5588,
- 210 5067-5590 and 5067-5589, Santa Clara, CA, USA). The pooled libraries were run on an Illumina
- 211 MiniSeq instrument using the MiniSeq Reagent MO Kit, (300 cycles) (Illumina Inc. San Diego,
- 212 CA, USA) for quality control and libraries balancing purposes. A new pool was made based on
- 213 the MiniSeq run results, quantified as described above and sequenced on an Illumina NovaSeq
- 214 6000 instrument (300 cycles) (Illumina Inc. San Diego, CA, USA), with a 1% phiX spike-in.
- 215 The sequencing data has been deposited in the SRA under Project number: PRJNA1319805

#### Sequence analysis

216

217

#### Sequence quality control and trimming

- 218 The quality of the raw reads was assessed using FastQC v. 0.11 (Babraham Bioinformatics).
- 219 Subsequently, the raw sequence reads were quality trimmed and filtered using Trimmomatic (v.

- 220 0.39) and the command "trimmomatic PE -threads 32 <output file names> LEADING:15
- TRAILING:15 SLIDINGWINDOW:4:15 MINLEN:36 HEADCROP:13". Upon trimming, the
- quality of the filtered reads was assessed using FastQC.

#### **Community composition**

223

229

242

- 224 Prokaryotic community composition was derived using PhyloFlash (V 3.3; (Gruber-Vodicka et al.
- 2020)) using the SILVA 138.1 DB as a reference. It is important to note that in the case of this
- study, the 16S rRNA read abundance represents a combination of relative abundance and activity
- as the data contains genomic DNA and cDNA.

#### 228 2.3.3 MetaG bioinfo

#### Metagenome-assembled genomes (MAG) assembly

- 230 Megahit v. 1.2.9 was used to assemble individual samples as well as a co-assembly of the entire
- dataset (28 samples). Binning was conducted using MaxBin2, and Metabat2, v. 2.12.12. Contig
- abundance files required for the binning tools were generated by mapping the raw data to the
- assembled contigs with MiniMap2, converting the SAM files into BAM files using SamTools, and
- 234 merging the resulting BAM files using the jgi summarize bam contig depths script included in
- 235 Metabat2. Bins were refined using MetaWrap and further dereplicated using dREP, v. 3.4.2 at 99%
- average nucleotide identity.
- Viral genomes and contigs were identified using Vibrant v1.2.1 (Kieft et al. 2020) applied to all
- assembled contigs above 1000 nucleotides. Information about the lifestyle a phage was in at the
- 239 time of sampling (lytic vs. lysogenic) is provided by the Vibrant tool, based on the contig structure
- in which the viral genes were found. Genome replication rates were calculated using iRep, v1.10
- 241 (Brown et al. 2016).

#### MAG analysis

- 243 The quality of obtained bins was analyzed using Checkm and Checkm2. Taxonomy was assigned
- to bins using GTDB-tk, v. 2.3.2 with database r214. The frequency of the different MAGs in the
- 245 mixed DNA-RNA data was evaluated using CoverM, v. 0.6.1
- 246 (<a href="https://github.com/wwood/CoverM">https://github.com/wwood/CoverM</a>). Annotation of the MAGs was done initially using Prokka,
- v. 1.14.5. Subsequently, all protein-coding open reading frames from the Prokka pipeline were

further annotated using the EggNog mapper (emapper v. 2.1.12), and mapped against the KEGG

249 database using BlastKoala and KofamKoala.

#### Gene expression quantification

251 The obtained sequence data contained sequences originating from both genomic DNA and

RNA. The subsequent calculations considered a fixed ratio between gene copy numbers in a given

MAG as the genome of an organisms is stable during the experiment. Therefore, any deviation

254 from that ratio would come from RNA data.

First, transcripts per kilobase million (TPM) values were calculated for the genes of each strain for each sample using Salmon, v. 1.10.1. Subsequently, a relative gene expression value was generated by dividing the TPM values of each protein by that of the *rpoB* gene (TPMr). The latter is a housekeeping gene for which minimal variation in expression is expected. The basal ratio between the expression of each gene and that of *rpoB* is unknown, therefore, for comparison purposes, the values for each gene were scaled separately for each *MAG* between 0 and 1, where 1 was the sample with the highest value for that particular gene. Zero values were treated as missing data rather than the lack of expression. As a control, the change in ratio between housekeeping genes was calculated and compared between the different treatments (Figure S2).

#### 2.4 Biogeochemical analyses

#### 2.4.1 Particulate organic carbon and nitrogen

All glassware was pre-combusted before use and rinsed with 1 N HCl and Milli-Q water after each sample. All plastic wares were rinsed with 1 N HCl and Milli-Q water and changed for each sample. Sample aliquots for particulate organic carbon (POC, 50-104 mL) were filtered onto pre-combusted 0.7 µm GF/F filters (25 mm filter diameter) under a low vacuum (<50mm Hg) and preserved at -20°C or in liquid nitrogen, respectively. Filters for particulate organic carbon and nitrogen (POC, PON) were analyzed as in (Raimbault et al. 2008) using a high combustion (1000°C) mass spectrometer (CN-Integra tracer-mass).

#### 2.5 Statistical analysis

- All statistical analyses were conducted in R (v4.x). All tests were two-tailed with  $\alpha = 0.05$ .
- Variance of the ratios (Figure 3a) between pressure treatments (TF-ATM vs TF-HP) was assessed
- using Levene's test (Fox and Weisberg (2018); car::leveneTest) and the Fligner-Killeen test (R
- 278 Core Team, 2023; stats::fligner.test), both robust approaches for testing heteroscedasticity
- 279 (Levene; Howard 1960; Fligner and Killeen 1976).
- The linear mixed-effects models (LME) was performed with pressure as a fixed effect and random
- intercepts for particle, gene, and taxon (lme4::lmer; Bates et al. 2015). From these models we
- extracted Best Linear Unbiased Predictors (BLUPs), which represent the estimated random effects
- 283 (i.e. how much each particle, gene, or taxon deviates from the global mean after accounting for
- 284 fixed effects). BLUPs were compared between treatments using Welch's t-tests. Model
- assumptions were verified using residual diagnostics, and analyses were repeated with both lme4
- and nlme (Pinheiro et al. 2025) to confirm robustness.

### 3. Results

288 3.1 MAG statistics.

287

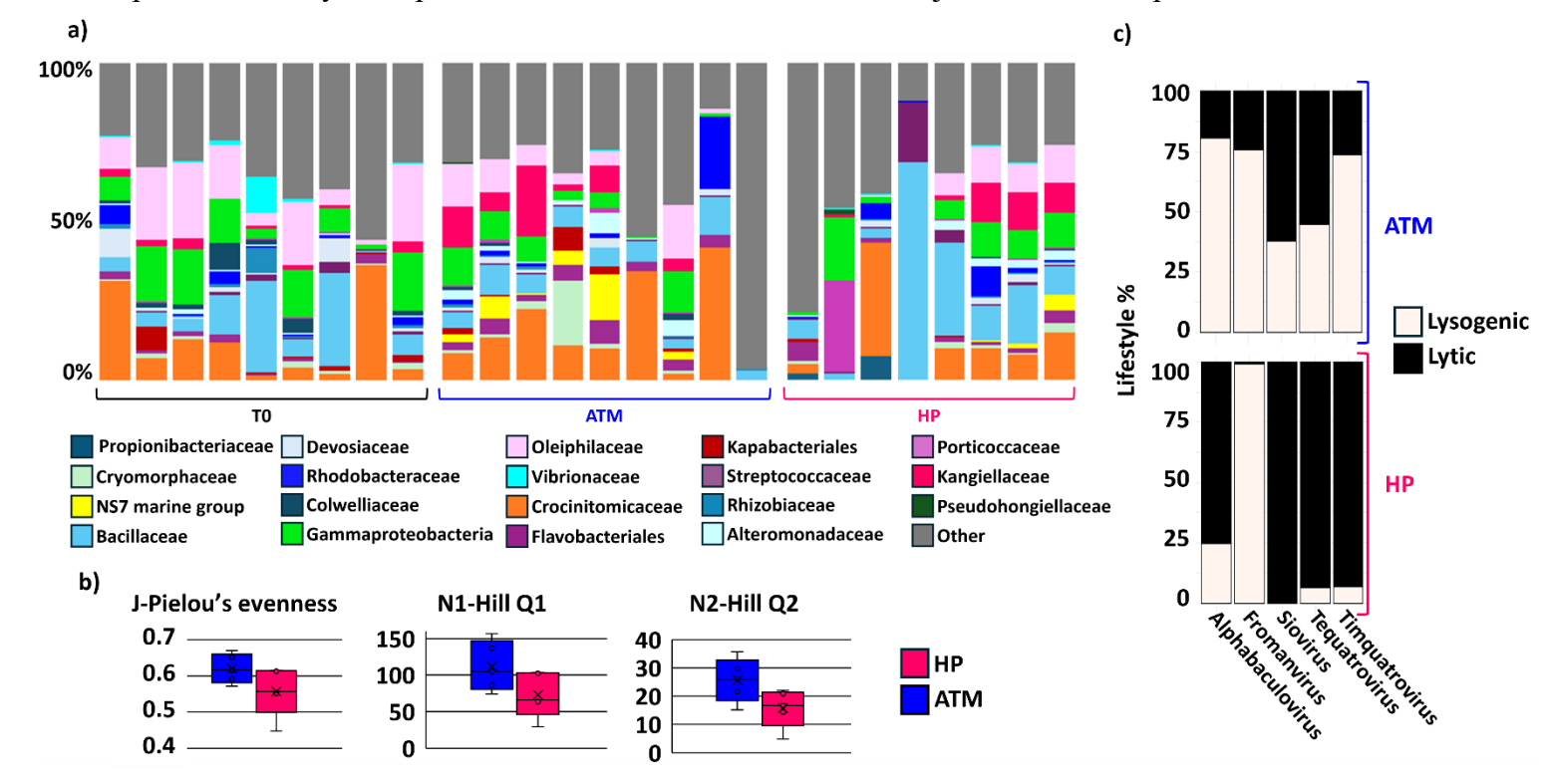
293

- A total of 287 MAGs (Metagenome Assembled Genomes) were obtained (**Table S1**) of which 92
- 290 had a completeness above 75 % and a contamination level below 5 %. These MAGs could be
- annotated to 15 different bacterial species, 5 of which in the phylum Bacteroidota, 9 in
- 292 Pseudomonadota (formerly Proteobacteria), and 1 in Bacillota (formerly Firmicutes).

#### 3.2 Effect of increased pressure on microbial community composition and diversity

- There is a large heterogeneity in the microbial community among individual particles, already at
- 295 the sequence frequency of bacterial families (Figure 1a). Notably, all of the families observed in
- 296 TF-ATM and TF-HP were also detected in T0 as expected (i.e. even if rare, they were already
- 297 present). Some families, including for instance Flavobacteriaceae, Crocinitomicaceae, and
- 298 Oleiphilaceae, were present on all particles; however, their relative abundances varied
- significantly,  $17.5\pm16\%$ ,  $10.3\pm10.4\%$  and  $5.8\pm6.0\%$ , respectively. Among the 20 most abundant
- families (**Figure 1a**), 14 for T0 and 13 for TF-ATM exhibited a standard deviation higher than the
- 301 average relative abundance across all analyzed individual particles. These high standard deviations
- underscore a significant variability at the single particle level. For TF-HP, only 3 families are in

this case however, 13 other families (still among the 20 most abundant) had low sequence frequencies (< 1%) across particles. Moreover, some families like the NS7 marine group were present in only one particle with a relative abundance of just 0.02%. Despite the inherent



heterogeneity of the particles, a discernible trend was observed across environmental conditions: particles in TF-HP exhibited a generally lower diversity compared to those in TF-ATM (p-value < 0.01; **Figure 1b**).

Figure 1: a) Relative abundance of the 20 most abundant prokaryotic families based on 16S rRNA reads before starting the experiment (T0), at the end of incubation with constant increase of pressure simulating the sink of particles (TF-HP) from the surface to 516m, and at the end without any pressure increase (TF-ATM). Each bar refers to one single particle; b) Diversity indices for prokaryotic diversity at increasing pressure (HP) and atmospheric pressure (ATM); c) Lifestyle percentage of various viruses found in TF-ATM vs. TF-HP. Differences between TF-ATM and TF-HP were statistically significant across all three diversity indices (p-value < 0.01).

One novel outcome of our data is the evaluation of a changing viral lifestyle with constantly increasing pressure (TF-HP). With the exception of *Fromanvirus*, we observe a general shift from a lysogenic state (or a balance between lysogenic and lytic forms) to a predominance of the lytic lifestyle at increasing pressure (**Figure 1c**). In TF-HP particles, the lytic forms can dominate with >90%, for instance, *Siovirus*, *Tequatrovirus*, and *Timquatrovirus* (99.6%, 93.7% and 93.3% respectively).

#### 3.4 Pressure induced stress

Comparing transcriptional activity across different individual particles colonized by different microorganisms in the absence of any reference genome remains difficult. Obtaining separate metagenomes and metatranscriptomes from individual particles is also not feasible due to the low organismic biomass. Therefore, our approach offers a compromise that allows an inter-particle comparative transcriptomic analysis for those microorganisms whose genome we could assemble from the obtained sequence data. We successfully identified 13 taxa (after dereplication) with metagenome-assembled genomes (MAGs) of sufficient quality to assess functional-to-housekeeping gene ratios (**Figure 2**).

All 13 taxa show a clear response to increasing pressure (**Figure 2a**). Whether the response leads to an up or down regulation is taxa dependent. Some, like PZK01-S or *Polaribacter*, exhibit a broad gene downregulation of cellular functions with the entire cellular machinery affected. In contrast, some taxa, such as GCA\_2720865 or *Croceibacter*, show gene upregulation across most cellular functions. Targeting genes, known to be involved in pressure-stress response (full list with references in **Table S2**), we found that these genes - identified in our MAGs - revealed a significant response to increasing pressure in our experiment (**Figure 2b**).

Calculated genome replication rates were significantly lower under pressure confirming an overall cellular stress (p-value of 0.0003 as described below). These rates have been previously shown to be a good proxy for growth rates and therefore indicators for stress-related growth inhibition (Korem et al. 2015; Brown et al. 2016). Genome replication rates had a median value of  $0.5 \pm 0.3$  in TF-ATM particles, but of only  $0.3 \pm 0.3$  in TF-HP (p-value of 0.0003; **Figure S3**).

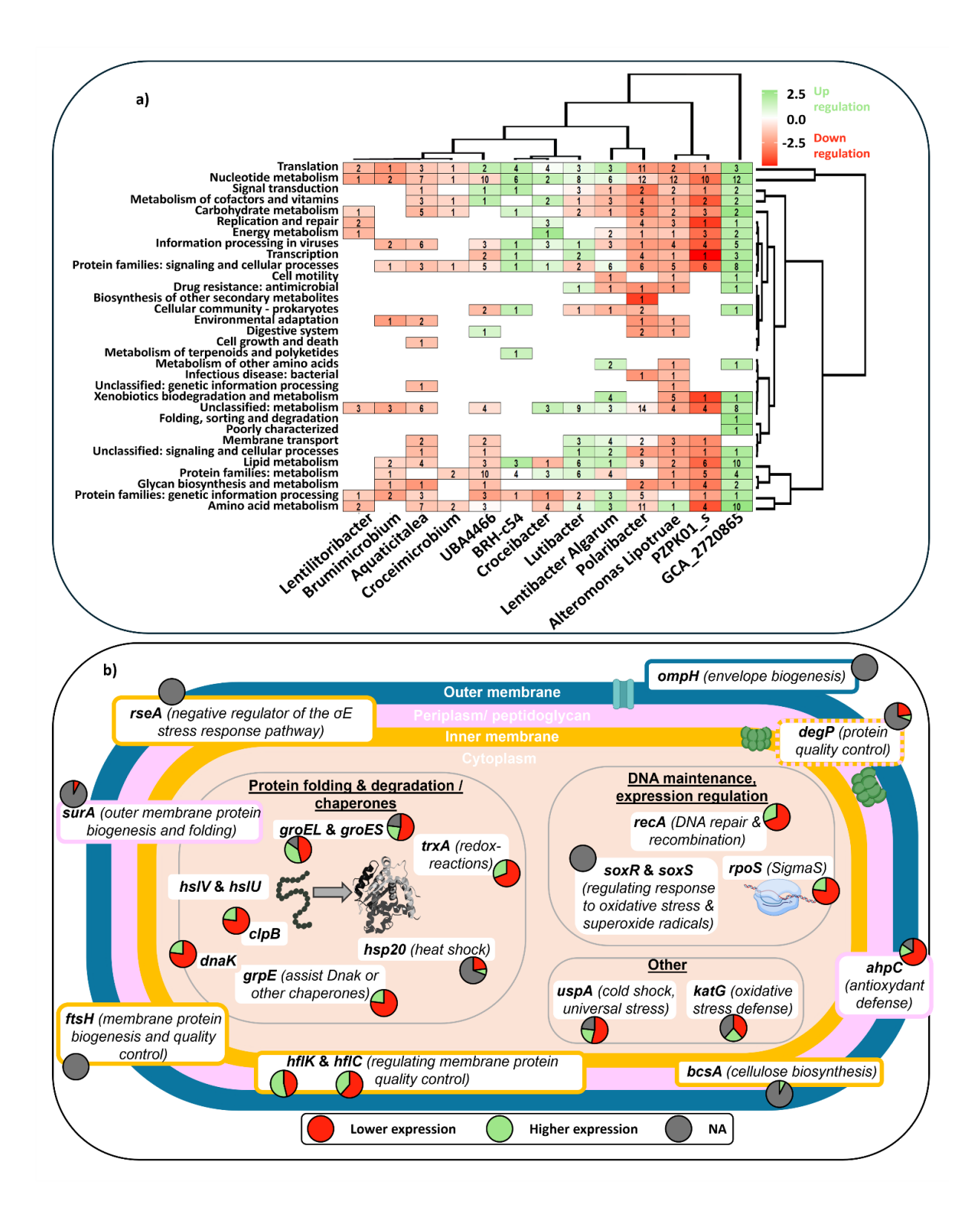
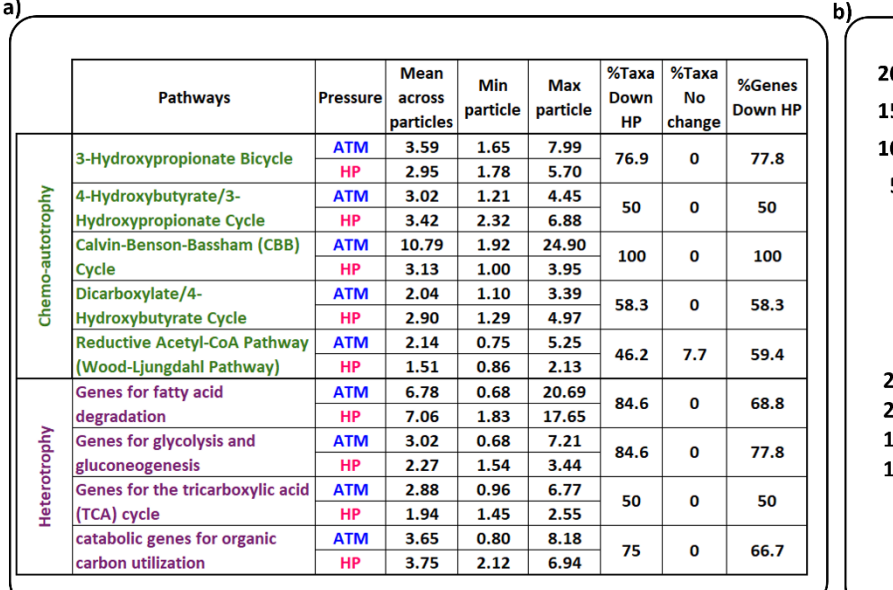


Figure 2: a) Overview of differential gene expression at KO function level 3, Log2-ratio of HP/ATM (a negative ratio (red) indicates downregulation at TF-HP compared to TF-ATM and conversely a positive ratio (green) indicates upregulation), numbers displayed = number of

genes used; b) Genes previously known to be differentially expressed as a result of pressure stress. Pies = proportion of taxa for which Log2-ratio of HP/ATM is higher than 1 (green) or lower (red). Known genes which could not be identified in our MAGs were included in the figure (grey) and marked as NA.

#### 3.5 Overall pressure effects on the mesopelagic carbon cycle

Particle heterogeneity was high, regardless of the metabolic pathway, whether heterotrophic or chemoautotrophic (**Figure 3a**). For instance, for taxon PZPK01, the relative expression of the gene *fadA* (involved in fatty acid degradation) showed a wide range, varying from 416.16 to 0.63 TPMr among single particles at TF-ATM. Similarly, for *Croceimicrobium*, the gene *accA* (part of the 3-Hydroxypropionate Bicycle) varied substantially from 0.64 to 74.55 at TF-HP. The highlighted heterogeneity within the same experimental condition is particularly compelling given that all particles were derived from the same roller tank and were exposed to the same initial prokaryotic community.



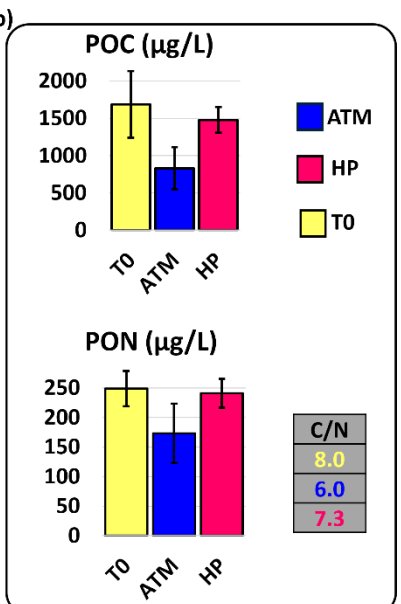


Figure 3: a) Summary of pressure effects on microbial metabolic pathways (Table S3 for the detailed list of genes used). For each pathway and pressure condition (TF-ATM or TF-HP), the table reports the mean, minimum, and maximum expression values across particles (normalized to rpoB), reflecting particle-level variability. Columns on taxonomic and functional response show the percentage of taxa with lower expression under high pressure (% taxa down under

HP), the percentage of taxa showing no change, and the percentage of gene-taxon combinations downregulated under high pressure. Together, these metrices highlight both particle-scale variability and within-pathway divergence in microbial responses to hydrostatic pressure.; b) Variability in measured biogeochemical parameters.

368

369

370

371

372

373

374

375

376

377

378

379

380 381

382

383

384

385

386

387

388

389

390

391

392

393

394

395

396

Expression trends across metabolic pathways showed that most taxa and gene—taxon combinations were downregulated under increasing pressure (HP), indicating a general suppressive effect on microbial activity (**Figure 3a**). This was especially clear for the Calvin-Benson-Bassham (CBB) cycle, where 100% of taxa and gene—taxon pairs decreased in expression at TF-HP. Despite variable particle-level means, the consistent downregulation at finer taxonomic and functional levels suggests that increase of pressure broadly inhibits the metabolic potential of surface-originating prokaryotes.

However, given the complexity of the dataset—with contributions from multiple genes, taxa, and individual particles—we sought to further explore whether the variability observed was structured or of more stochastic in nature. The variance of the ratio (Figure 3a) was slightly, but significantly higher at TF-ATM than TF-HP (Levene's or Fligner-Killeen tests p-value < 0.01; both ideal to quantify stochasticity as variabilities). This suggests heteroscedasticity in the data (non-uniform variability). The high variability due to different taxa and gene combinations could introduce substantial heterogeneity and mask any effect of pressure on stochasticity in the system. To assess random effects without this masking, we performed a Mixed-Effects Model (LME) and nested and partitioned the random effects at levels of particles, genes and taxa. No significant difference was observed in the mean random effects between pressure levels, as indicated by a p-value of 1 when comparing random effects via t-test. This analysis provides evidence that increasing pressure affects variability without significantly altering the underlying random effects across the nested factors. The observed difference in variances suggests that increasing pressure restricts the range of microbial carbon utilization by surface-originating prokaryotes when compared to atmospheric pressure. Yet, as the mixed-effects model showed no significant differences in random effects between pressure, hydrostatic pressure may affect the spreading of cellular responses, but does not consistently shift carbon utilization across individual particles. Thus, our results suggest that hydrostatic pressure mainly acts by restricting the variability of responses across taxa, rather than

- producing a uniform shift in carbon usage, indicating that while pressure narrows the range of variability, intrinsic stochasticity continues to shape system-level outcomes.
- 399 No difference was observed for particulate organic carbon (POC) or nitrogen (PON)
- 400 concentrations in the high-pressure incubation experiments (Figure 3b). In contrast, there was a
- significant decrease in both POC and PON concentrations at atmospheric pressure (Figure 3b).

### 4. Discussion

397

398

402

410

411

412

413

414

415

416

417

418

419

420

421

422

423

424

- 403 Prokaryotes colonizing particles before they sink primarily originate from surface environments.
- We therefore anticipated that the increasing pressure on sinking particles induces general cellular
- stress for initial particle colonizers. We hypothesized that this stress could lead to diminished
- 406 expression of genes linked to cellular/metabolic processes. This mechanism could explain
- 407 observed reductions in organic matter degradation on particles under high pressure. This
- 408 experiment enables us to test this hypothesis. Furthermore, we aimed to explore the heterogeneity
- among aggregates, a phenomenon for which compelling evidence is only beginning to emerge.

### 4.1 Insights into variability and taxa-dependent pressure responses

Our study provides insights into the variability within particle-associated microbial communities and their responses to increasing hydrostatic pressure. Unlike previous studies that broadly examined community-level responses (Boeuf et al. 2019; Poff et al. 2021), we reveal how inherent heterogeneity obscures global gene expression trends between TF-ATM and TF-HP conditions for surface-originating prokaryotes. This variability poses a significant challenge in linking molecular data to biogeochemical processes, particularly as taxa-dependent responses dominate over uniform functional trends. By analyzing taxa-specific responses, we demonstrate that stress of surface-originating prokaryotes under increasing pressure is tightly linked to physiological and genomic characteristics of individual taxa, a finding consistent with emerging evidence for stress-responses other than to pressure (Dawan and Ahn 2022). For example, while genes involved in stress responses, protein folding, and DNA repair—such as hflC, hflK, and bcsA—are often upregulated under stress due to increase of hydrostatic pressure in non-piezophile bacteria (Nikparvar et al. 2021; Malas et al. 2024), our data reveal certain exceptions to these patterns. We were able to investigate 13 dominant species on our particles. While the diversity on the particles was higher,

the rarer species were either not present on sufficient particles or their genome completeness was not high enough to allow for a reliable gene expression analysis using the ratio to housekeeping genes. However, most of the dominant surface water taxa, we have analyzed appear to be sensitive to increasing hydrostatic pressure. This is consistent with known characteristics of piezosensitive organisms, which often exhibit widespread functional decline under pressure stress (Oger and Jebbar 2010; Marietou and Bartlett 2014). This leads to reduced metabolic activity and impaired growth (Grossart and Gust 2009). This is also consistent with the decrease in diversity we have observed in this particle sinking simulation and previous one (Tamburini et al. 2021). In situ studies similarly reported a decline in particle-associated diversity from the surface to 500m (Thiele et al. 2015; Baumas et al. 2021). In contrast, piezo-tolerant or potentially piezophilic organisms are capable of maintaining or enhancing cellular processes under increasing pressure, consistent with findings in other pressure-adapted microbes (Yayanos 1995; Oger and Jebbar 2010; Tamburini et al. 2013). Piezophilic taxa have indeed been reported on particles, but in the bathypelagic, depths well beyond the range of our experiment (Boeuf et al. 2019; Preston et al. 2020; Poff et al. 2021), suggesting that within the upper mesopelagic (to 516 m) the active colonizers are more likely piezotolerant rather than true piezophiles. Baumas et al. (2021) found that diversity correlated to heterotrophic activity in free-living but not in particle-associated prokaryotes. This might be because bulk measurements conceal particle-to-particle heterogeneity, where different taxa with distinct pressure responses coexist.

Heterogeneity among individual particles has mainly been evidenced in terms of microbial diversity and such studies are still too scarce to generalize (Bizic-Ionescu et al. 2018; Zäncker et al. 2019; Baumas et al. 2023b; Stief et al. 2023). Our work further highlights a novel dimension of heterogeneity: even within individual particles of the same origin, microbial diversity and gene expression exhibit significant variability. This variability could thus be magnified when considering *in situ* particles with diverse origins, compositions, and histories. Such findings underscore the need for refined methodologies capable of accounting for this obvious stochasticity in models of microbial community behavior and functional response (De Vrieze et al. 2020). By doing so, our study sets a new benchmark for understanding microbial contributions to carbon cycling.

#### 4.2 Pressure-driven viral dynamics

425

426

427

428

429

430

431

432

433

434

435

436

437

438

439

440

441

442

443

444

445

446

447

448

449

450

451

452

453

Our study identifies a notable shift from lysogenic to lytic viral forms under increasing pressure.

This discovery highlights how environmental stress, such as hydrostatic pressure, can trigger viral

life-cycle changes—a phenomenon consistent with previous findings from (Weinbauer 2004;

Danovaro et al. 2011). Such shifts may represent a survival strategy where viruses exploit stressed

host cells, leading to increased replication and host cell lysis. This dynamic is particularly relevant

in the context of marine aggregates, which are known hotspots for virus-host interactions

461 (Riemann and Grossart 2008; Bizic-Ionescu et al 2018).

The predominance of lytic forms with the increase of pressure could have significant implications for prokaryotic community structure and function, potentially leading to increased mortality of host organisms (infected prokaryotes included) and altering nutrient cycling within these ecosystems as shown for other environmental stress sources (Wilhem and Suttle 1999; Breitbart 2012). Increased prokaryote mortality due to viral lysis could reduce the role of these bacteria in organic matter degradation, slowing down the breakdown of POC (Gao et al. 2022). In parallel, the release of cell contents from lysed cells contributes to the pool of dissolved organic carbon (DOC), leading to faster mineralization of organic matter (Middelboe and Jørgensen 2006; Zhang et al. 2018). While these contradicting effects require further quantification, accounting for the effects of pressure in models is likely to improve the estimation of carbon export to the deep ocean. Recent global analyses have shown that viral community composition itself can be a strong predictor of carbon export efficiency (Kaneko et al. 2020), highlighting the broad regulatory role of viruses across hosts.

Further investigation into these mechanisms (specifically abundance and fluxes) could deepen our understanding of microbial ecology on particles, and thus, associated biogeochemical cycles. For instance, Jasna et al. (2018) found that preferential infections of prokaryotic morphological populations with respect to seasons can have a strong and variable impact on the carbon and energy flow of an estuarine ecosystem. We could imagine the same type of investigation for the water column with increasing pressure and changing types of POC (involving intrinsically different diversity of attached to sinking particles prokaryotes). In any case, our results suggest that viral lysis plays a regulatory role in the carbon cycle on particles. This regulatory mechanism must be incorporated into models of carbon flux, as it has the potential to significantly alter estimates of carbon sequestration under changing ocean conditions.

#### 4.3 Metabolic pathway disruptions and their implications on the carbon cycle

485

486

487

488

489

490

491

492

493

494

495

496

497

498

499

500

501

502

503 504

505

506

507

508

509

510

511

512

513

514

Increasing hydrostatic pressure leads to changes in gene expression of both heterotrophic and autotrophic pathways of surface-originating prokaryotes, thus likely affecting the carbon flux (Table S3). We observed pronounced downregulation under pressure stress in glycolysis, fatty acid degradation, and the TCA cycle (mostly heterotrophic), as well as in the reductive TCA cycle and the Calvin-Benson-Bassham cycle (chemolithoautrophy) (Figure 3a). Prokaryotes exhibit a diverse array of metabolic strategies, enabling them to access and process a large variety of organic molecules that are found (also) in marine snow (Simon et al. 2002). This trait is vital, as the flux of organic carbon from marine snow - via activities of attached prokaryotes - serves as the principal carbon source for the mesopelagic zone and represents a key vector for carbon sequestration (Baumas et al. 2021). While these strategies predominantly involve heterotrophic activities, the potential role of dark CO<sub>2</sub> fixation in the carbon cycle is often overlooked though it is important as well (Arandia-Gorostidi et al. 2024; Le Coq et al. accepted). Large-scale expeditions such as Tara Oceans and Malaspina have analyzed suspended particle-sized fractions using metagenomics and metatranscriptomics - including functional genes and CAZymes (Vernette et al. 2022). Nevertheless, high-resolution studies of marine particles remain limited, particularly given the complexity of these systems (reviewed in Baumas and Bizic 2024), making it challenging to directly link pathway activity to specific particles. Even more so, those studies focusing on individual particles, enable us to understand the degree of heterogeneity in activity as compared to that in community composition.

Unlike earlier studies employing sinking speeds between 100 and 200 m/day as experimental compromises (Tamburini et al. 2006, 2009, 2021; Grossart and Gust 2009; Riou et al. 2018; Franco-Cisterna et al. 2024), we simulated slower, representative of the sinking rates of the particles used. Despite these moderate pressures change (0.1 to 5.2 MPa simulating the sink between the surface and 516 m), we observed significant changes in microbial gene expressions, shifts in community composition, and decrease of organic matter degradation reinforcing the importance of hydrostatic pressure as a critical factor shaping microbial ecology during particle sinking.

Our results also extend the scope of metatranscriptomics analyses by focusing on individual particles to capture intra-particle heterogeneity that is masked in bulk community analyses (e.g.

Bizic-Ionescu et al. 2018). This fine-scale resolution shows that microbial activity is not always predictable from community composition alone, and that different particles - despite originating from the same environment - harbor distinct functional profiles. This heterogeneity between particles raised the question of both, stochastic colonization and metabolic flexibility as well, highlighting the potential ability of microorganisms to dynamically adjust their metabolic pathways in response to varying conditions between different particles and pressure. By integrating these findings, our study is fundamental for disentangling how specific environmental pressures - such as hydrostatic pressure or particle composition - select for distinct metabolic strategies, and how these shifts scale up to influence microbial contributions to biogeochemical cycles.

### 5. Conclusion

Our findings challenge long-held assumptions of a uniform surface-originating prokaryotic response to pressure stress and highlight the need for new experimental and analytic methodologies to account for high variability and taxa-dependent dynamics. Our bioinformatic approach allowed us to simultaneously investigate identify the dominant organism on particles, as well as resolve their transcriptional response to pressure. While this approach does not generate an absolute transcriptional profile, it offers a solution for low biomass samples, where separate metagenomic and metatranscriptomics data cannot be done. Furthermore, it provides transcriptional information also on genes that could not have been accurately classified taxonomically in the absence of a MAG from the same sample. The discovery of pressure-regulated viral life cycles and their cascading effects on carbon cycling adds a new vector to the viral shunt that goes beyond "killing the winner". However, the ambiguous effects of pressure induced viral lysis call for quantification through targeted experiments before these could be incorporated into ocean carbon models.

Previous studies reported broad, global pressure effects at much greater depths than shown in our study (Oger and Jebbar 2010; Tamburini et al. 2013; Amano et al. 2022). We revealed that pressure effects already take place in the upper mesopelagic region of the ocean. The uncoordinated nature of the pressure effects at these depths is masked by bulk sampling and has therefore remained undetected so far. Our controlled setup provides an unprecedented, fine-scale view (by taxon and by particle), allowing us to detect these effects.

Our findings suggest that when accounted for, pressure driven changes in microbial function and community, alongside inter-particle variability should improve our ability to model the fate of organic matter in the ocean and its contribution to long-term carbon storage -even under current and future oceanic changes. By bridging gaps in knowledge and introducing novel perspectives, our study paves the way for future investigations into the complex interplay between microbial ecology, viral dynamics, and carbon fluxes in marine systems.

### **Author contribution**

CT, HPG and MB supervised the work. CB, MG and CT conceptualized (as well as HPG) and performed the sinking simulation experiment. MB, DI, and CB developed and carried out the processes from nucleic acid extraction to library preparation. DI and MB conceptualized and conducted the bioinformatic analysis. All authors contributed to the writing of the manuscript.

## Acknowledgement

We thank the crew and officers of the Tethys II for their help during the PARTY cruise. The project leading to this publication has received funding from European FEDER Fund under project 1166-39417. The project leading to this publication has received funding from Excellence Initiative of Aix-Marseille University – A\*MIDEX, a French "Investissements d'Avenir" programme. The authors thank the SAM facilities and the PEB plateform of MIO for providing the technical means and skills of its personnel and making available equipment and protocols. We also thank Fatima Ezzahra Ababou for measuring the TEP and CSP concentrations, even though the data could not ultimately be used.

# **Competing interests**

The authors declare that they have no conflict of interest.

### References

567	Allen, E. E., D. Facciotti, and D. H. Bartlett. 1999. Monounsaturated but Not Polyunsaturated Fatty
568	Acids Are Required for Growth of the Deep-Sea BacteriumPhotobacterium profundum SS9
569	at High Pressure and Low Temperature. Applied and Environmental Microbiology 65: 1710–
570	1720. doi:10.1128/AEM.65.4.1710-1720.1999
571	Amano, C., Z. Zhao, E. Sintes, T. Reinthaler, J. Stefanschitz, M. Kisadur, M. Utsumi, and G. J. Herndl.
572	2022. Impact of hydrostatic pressure on organic carbon cycling of the deep-sea
573	microbiome. 2022.03.31.486587. doi:10.1101/2022.03.31.486587
574	Arandia-Gorostidi, N., A. L. Jaffe, A. E. Parada, B. J. Kapili, K. L. Casciotti, R. S. R. Salcedo, C. M. J.
575	Baumas, and A. E. Dekas. 2024. Urea assimilation and oxidation support activity of
576	phylogenetically diverse microbial communities of the dark ocean. The ISME Journal
577	wrae230. doi:10.1093/ismejo/wrae230
578	Bartlett, D. H. 2002. Pressure effects on in vivo microbial processes. Biochim Biophys Acta <b>1595</b> :
579	367–381. doi:10.1016/s0167-4838(01)00357-0
580	Bartlett, D. H., F. M. Lauro, and E. A. Eloe. 2007. Microbial Adaptation to High Pressure, p. 331–348.
581	In Physiology and Biochemistry of Extremophiles. John Wiley & Sons, Ltd.
582	Bates, D., M. Mächler, B. Bolker, and S. Walker. 2015. Fitting Linear Mixed-Effects Models Using
583	lme4. Journal of Statistical Software 67: 1–48. doi:10.18637/jss.v067.i01
584	Baumas, C., and M. Bizic. 2024. A focus on different types of organic matter particles and their
585	significance in the open ocean carbon cycle. Progress in Oceanography 224: 103233.
586	doi:10.1016/j.pocean.2024.103233
587	Baumas, C., R. Fuchs, M. Garel, JC. Poggiale, L. Memery, F. A. C. Le Moigne, and C. Tamburini.
588	2023a. Reconstructing the ocean's mesopelagic zone carbon budget: sensitivity and
589	estimation of parameters associated with prokaryotic remineralization. Biogeosciences 20:
590	4165–4182. doi:10.5194/bg-20-4165-2023

591	Baumas, C. M. J. and others. 2021. Mesopelagic microbial carbon production correlates with
592	diversity across different marine particle fractions. The ISME Journal 15: 1695–1708.
593	doi:10.1038/s41396-020-00880-z
594	Baumas, C. M. J. and others. 2023b. A novel method to sample individual marine snow particles for
595	downstream molecular analyses. Limnology and Oceanography: Methods <b>n/a</b> .
596	doi:10.1002/lom3.10590
597	Bizic, M., D. Ionescu, S. Wang, F. Zhang, and Y. Shaked. 2024. Phenotypic variability between
598	closely related Trichodesmium strains as a means to making the most out of
599	heterogeneous microenvironments. 2024.05.22.595369. doi:10.1101/2024.05.22.595369
600	Bizic-Ionescu, M., D. Ionescu, and HP. Grossart. 2018. Organic Particles: Heterogeneous Hubs
601	for Microbial Interactions in Aquatic Ecosystems. Frontiers in Microbiology <b>9</b> : 1–15.
602	doi:10.3389/fmicb.2018.02569
603	Boeuf, D. and others. 2019. Biological composition and microbial dynamics of sinking particulate
604	organic matter at abyssal depths in the oligotrophic open ocean. Proceedings of the
605	National Academy of Sciences of the United States of America 116.
606	doi:10.1073/pnas.1903080116
607	Breitbart, M. 2012. Marine Viruses: Truth or Dare. Annual Review of Marine Science <b>4</b> : 425–448.
608	doi:10.1146/annurev-marine-120709-142805
609	Brown, C. T., M. R. Olm, B. C. Thomas, and J. F. Banfield. 2016. Measurement of bacterial
610	replication rates in microbial communities. Nat Biotechnol <b>34</b> : 1256–1263.
611	doi:10.1038/nbt.3704
612	Burd, A. B. and others. 2010. Assessing the apparent imbalance between geochemical and
613	biochemical indicators of meso- and bathypelagic biological activity: What the @\$#! is

614	wrong with present calculations of carbon budgets? Deep-Sea Research Part II: Topical
615	Studies in Oceanography 1557–1571. doi:10.1016/j.dsr2.2010.02.022
616	Danovaro, R., C. Corinaldesi, A. Dell'anno, J. A. Fuhrman, J. J. Middelburg, R. T. Noble, and C. A.
617	Suttle. 2011. Marine viruses and global climate change. FEMS Microbiol Rev <b>35</b> : 993–1034.
618	doi:10.1111/j.1574-6976.2010.00258.x
619	Dawan, J., and J. Ahn. 2022. Bacterial Stress Responses as Potential Targets in Overcoming
620	Antibiotic Resistance. Microorganisms 10: 1385. doi:10.3390/microorganisms10071385
621	De Vrieze, J., T. De Mulder, S. Matassa, J. Zhou, L. T. Angenent, N. Boon, and W. Verstraete. 2020.
622	Stochasticity in microbiology: managing unpredictability to reach the Sustainable
623	Development Goals. Microb Biotechnol <b>13</b> : 829–843. doi:10.1111/1751-7915.13575
624	DeLong, E. F., and A. A. Yayanos. 1985. Adaptation of the Membrane Lipids of a Deep-Sea
625	Bacterium to Changes in Hydrostatic Pressure. Science 228: 1101–1103.
626	doi:10.1126/science.3992247
627	Dong, S., A. V. Subhas, N. E. Rollins, J. D. Naviaux, J. F. Adkins, and W. M. Berelson. 2018. A kinetic
628	pressure effect on calcite dissolution in seawater. Geochimica et Cosmochimica Acta 238:
629	411–423. doi:10.1016/j.gca.2018.07.015
630	Fligner, M. A., and T. J. Killeen. 1976. Distribution-Free Two-Sample Tests for Scale. Journal of the
631	American Statistical Association <b>71</b> : 210–213. doi:10.1080/01621459.1976.10481517
632	Fox, J., and S. Weisberg. 2018. An R Companion to Applied Regression, SAGE Publications.
633	Franco-Cisterna, B., P. Stief, and R. N. Glud. 2024. Hydrostatic pressure impedes the degradation
634	of sinking copepod carcasses and fecal pellets M. Koski [ed.]. Journal of Plankton Research
635	fbae002. doi:10.1093/plankt/fbae002

636	Gao, Y., Y. Lu, J. A. J. Dungait, J. Liu, S. Lin, J. Jia, and G. Yu. 2022. The "Regulator" Function of
637	Viruses on Ecosystem Carbon Cycling in the Anthropocene. Front. Public Health 10.
638	doi:10.3389/fpubh.2022.858615
639	Garcia, H. E., and L. I. Gordon. 1992. Oxygen solubility in seawater: Better fitting equations.
640	Limnology and Oceanography <b>37</b> : 1307–1312. doi:10.4319/lo.1992.37.6.1307
641	García-Martín, E. E., S. McNeill, P. Serret, and R. J. G. Leakey. 2014. Plankton metabolism and
642	bacterial growth efficiency in offshore waters along a latitudinal transect between the UK
643	and Svalbard. Deep Sea Research Part I: Oceanographic Research Papers <b>92</b> : 141–151.
644	doi:10.1016/j.dsr.2014.06.004
645	Garel, M., P. Bonin, S. Martini, S. Guasco, M. Roumagnac, N. Bhairy, F. Armougom, and C.
646	Tamburini. 2019. Pressure-Retaining Sampler and High-Pressure Systems to Study Deep-
647	Sea Microbes Under In Situ Conditions. Frontiers in Microbiology 10: 453.
648	doi:10.3389/FMICB.2019.00453
649	Grossart, H. P., and G. Gust. 2009. Hydrostatic pressure affects physiology and community
650	structure of marine bacteria during settling to 4000 m: An experimental approach. Marine
651	Ecology Progress Series <b>390</b> : 97–104. doi:10.3354/meps08201
652	Grossi, V. and others. 2010. Hydrostatic pressure affects membrane and storage lipid
653	compositions of the piezotolerant hydrocarbon-degrading Marinobacter
654	hydrocarbonoclasticus strain #5. Environmental Microbiology <b>12</b> : 2020–2033.
655	doi:10.1111/j.1462-2920.2010.02213.x
656	Gruber-Vodicka, H. R., B. K. B. Seah, and E. Pruesse. 2020. phyloFlash: Rapid Small-Subunit rRNA
657	Profiling and Targeted Assembly from Metagenomes M. Arumugam [ed.]. mSystems 5:
658	e00920-20. doi:10.1128/mSystems.00920-20

659	Guillard, R. R. L. 1975. Culture of Phytoplankton for Feeding Marine Invertebrates, p. 29–60. <i>In</i> W.L.
660	Smith and M.H. Chanley [eds.], Culture of Marine Invertebrate Animals: Proceedings — 1st
661	Conference on Culture of Marine Invertebrate Animals Greenport. Springer US.
662	Guillard, R. R. L., and P. E. Hargraves. 1993. Stichochrysis immobilis is a diatom, not a
663	chrysophyte. Phycologia <b>32</b> : 234–236. doi:10.2216/i0031-8884-32-3-234.1
664	Jasna, V., A. S. P. Ram, A. Parvathi, and T. Sime-Ngando. 2018. Differential impact of lytic viruses
665	on prokaryotic morphopopulations in a tropical estuarine system (Cochin estuary, India).
666	PLOS ONE <b>13</b> : e0194020. doi:10.1371/journal.pone.0194020
667	de Jesus Mendes, P. A., L. Thomsen, B. Holscher, H. C. de Stigter, and G. Gust. 2007. Pressure
668	effects on the biological degradation of organo-mineral aggregates in submarine canyons.
669	Marine Geology <b>246</b> : 165–175. doi:10.1016/j.margeo.2007.05.012
670	Kaneko, H. and others. 2020. Eukaryotic virus composition can predict the efficiency of carbon
671	export in the global ocean. iScience <b>24</b> : 102002. doi:10.1016/j.isci.2020.102002
672	Kieft, K., Z. Zhou, and K. Anantharaman. 2020. VIBRANT: automated recovery, annotation and
673	curation of microbial viruses, and evaluation of viral community function from genomic
674	sequences. Microbiome 8: 90. doi:10.1186/s40168-020-00867-0
675	Kish, A., P. L. Griffin, K. L. Rogers, M. L. Fogel, R. J. Hemley, and A. Steele. 2012. High-pressure
676	tolerance in Halobacterium salinarum NRC-1 and other non-piezophilic prokaryotes.
677	Extremophiles <b>16</b> : 355–361. doi:10.1007/s00792-011-0418-8
678	Korem, T. and others. 2015. Growth dynamics of gut microbiota in health and disease inferred from
679	single metagenomic samples. Science <b>349</b> : 1101–1106. doi:10.1126/science.aac4812
680	Kwon, E. Y., F. Primeau, and J. L. Sarmiento. 2009. The impact of remineralization depth on the air-
681	sea carbon balance. Nature Geosci <b>2</b> : 630–635. doi:10.1038/ngeo612

682	Levene; Howard. 1960. Robust tests for equality of variances. contributions to probability and
683	statistics 278–292.
684	Liu, Y., M. Zeng, Z. Xie, D. Ning, J. Zhou, X. Yu, R. Liu, and L. Zhang. 2022. Microbial Community
685	Structure and Ecological Networks during Simulation of Diatom Sinking. 1–20.
686	Malas, J., D. C. Russo, O. Bollengier, M. J. Malaska, R. M. C. Lopes, F. Kenig, and D. R. Meyer-
687	Dombard. 2024. Biological functions at high pressure: transcriptome response of
688	Shewanella oneidensis MR-1 to hydrostatic pressure relevant to Titan and other icy ocean
689	worlds. Front. Microbiol. <b>15</b> . doi:10.3389/fmicb.2024.1293928
690	Marietou, A., and D. H. Bartlett. 2014. Effects of High Hydrostatic Pressure on Coastal Bacterial
691	Community Abundance and Diversity. Appl Environ Microbiol 80: 5992–6003.
692	doi:10.1128/AEM.02109-14
693	Martin, A. and others. 2020. The oceans' twilight zone must be studied now, before it is too late.
694	Nature. doi:10.1038/d41586-020-00915-7
695	McNeil, C. L., and E. A. D'Asaro. 2014. A calibration equation for oxygen optodes based on physical
696	properties of the sensing foil. Limnology and Oceanography: Methods 12: 139–154.
697	doi:10.4319/lom.2014.12.139
698	Mendes, P. A. de J., and L. Thomsen. 2012. Effects of Ocean Acidification on the Ballast of Surface
699	Aggregates Sinking through the Twilight Zone. PLOS ONE <b>7</b> : e50865.
700	doi:10.1371/journal.pone.0050865
701	Middelboe, M., and N. O. G. Jørgensen. 2006. Viral lysis of bacteria: an important source of
702	dissolved amino acids and cell wall compounds. Journal of the Marine Biological
703	Association of the United Kingdom <b>86</b> : 605–612. doi:10.1017/S0025315406013518
704	Mullane, K. K., M. Nishiyama, T. Kurihara, and D. H. Bartlett. 2023. Compounding deep sea physical
705	impacts on marine microbial motility. Front. Mar. Sci. 10. doi:10.3389/fmars.2023.1181062

706	Nikparvar, B. and others. 2021. Analysis of temporal gene regulation of Listeria monocytogenes		
707	revealed distinct regulatory response modes after exposure to high pressure processing.		
708	BMC Genomics <b>22</b> : 266. doi:10.1186/s12864-021-07461-0		
709	Oger, P. M., and M. Jebbar. 2010. The many ways of coping with pressure. Res Microbiol <b>161</b> : 799–		
710	809. doi:10.1016/j.resmic.2010.09.017		
711	Parekh, P., S. Dutkiewicz, M. J. Follows, and T. Ito. 2006. Atmospheric carbon dioxide in a less dusty		
712	world. Geophysical Research Letters 33: L03610. doi:10.1029/2005GL025098		
713	Passow, U., and T. Weber. 2025. The biological carbon pump, p. 333–369. <i>In</i> Treatise on		
714	Geochemistry. Elsevier.		
715	Pinheiro, J., D. Bates, and R Core Team. 2025. nlme: Linear and Nonlinear Mixed Effects Models.		
716	3.1-168. doi:10.32614/CRAN.package.nlme		
717	Poff, K. E., A. O. Leu, J. M. Eppley, D. M. Karl, and E. F. DeLong. 2021. Microbial dynamics of		
718	elevated carbon flux in the open ocean's abyss. Proceedings of the National Academy of		
719	Sciences <b>118</b> : e2018269118. doi:10.1073/pnas.2018269118		
720	Preston, C. M., C. A. Durkin, and K. M. Yamahara. 2020. DNA metabarcoding reveals organisms		
721	contributing to particulate matter flux to abyssal depths in the North East Pacific ocean.		
722	Deep Sea Research Part II: Topical Studies in Oceanography 173: 104708.		
723	doi:10.1016/j.dsr2.2019.104708		
724	Raimbault, P., N. Garcia, and F. Cerutti. 2008. Distribution of inorganic and organic nutrients in the		
725	South Pacific Ocean − evidence for long-term accumulation of organic matter in		
726	nitrogen-depleted waters. Biogeosciences <b>5</b> : 281–298. doi:10.5194/bg-5-281-2008		
727	Riemann, L., and HP. Grossart. 2008. Elevated Lytic Phage Production as a Consequence of		
728	Particle Colonization by a Marine Flavobacterium (Cellulophaga Sp.). Microbial Ecology <b>56</b> :		
729	505–512.		

730	Riou, V. and others. 2018. Biodegradation of Emiliania huxleyi aggregates by a natural
731	Mediterranean prokaryotic community under increasing hydrostatic pressure. Progress in
732	Oceanography <b>163</b> : 271–281. doi:10.1016/j.pocean.2017.01.005
733	Siegel, D. A., T. DeVries, I. Cetinić, and K. M. Bisson. 2023. Quantifying the Ocean's Biological
734	Pump and Its Carbon Cycle Impacts on Global Scales. Annu. Rev. Mar. Sci. 15: annurev-
735	marine-040722-115226. doi:10.1146/annurev-marine-040722-115226
736	Simon, M., H. Grossart, B. Schweitzer, and H. Ploug. 2002. Microbial ecology of organic aggregates
737	in aquatic ecosystems. Aquatic Microbial Ecology 28: 175–211. doi:10.3354/ame028175
738	Smith, D. C., M. Simon, A. L. Alldredge, and F. Azam. 1992. Intense hydrolytic enzyme activity on
739	marine aggregates and implications for rapid particle dissolution. Nature <b>359</b> : 139–142.
740	doi:10.1038/359139a0
741	Stief, P., M. Elvert, and R. N. Glud. 2021. Respiration by "marine snow" at high hydrostatic
742	pressure: Insights from continuous oxygen measurements in a rotating pressure tank.
743	Limnol Oceanogr <b>66</b> : 2797–2809. doi:10.1002/lno.11791
744	Stief, P., C. Schauberger, K. W. Becker, M. Elvert, J. P. Balmonte, B. Franco-Cisterna, M. Middelboe
745	and R. N. Glud. 2023. Hydrostatic pressure induces transformations in the organic matter
746	and microbial community composition of marine snow particles. Commun Earth Environ 4:
747	1–14. doi:10.1038/s43247-023-01045-4
748	Tamburini, C. and others. 2009. Effects of hydrostatic pressure on microbial alteration of sinking
749	fecal pellets. Deep Sea Research Part II: Topical Studies in Oceanography <b>56</b> : 1533–1546.
750	doi:10.1016/j.dsr2.2008.12.035
751	Tamburini, C. and others. 2021. Increasing Hydrostatic Pressure Impacts the Prokaryotic Diversity
752	during Emiliania huxleyi Aggregates Degradation. Water <b>13</b> : 2616. doi:10.3390/w13192616

753	Tamburini, C., M. Boutrif, M. Garel, R. R. Colwell, and J. W. Deming. 2013. Prokaryotic responses to
754	hydrostatic pressure in the ocean - a review. Environmental Microbiology <b>15</b> : 1262–1274.
755	doi:10.1111/1462-2920.12084
756	Tamburini, C., J. Garcin, G. Grégori, K. Leblanc, P. Rimmelin, and D. L. Kirchman. 2006. Pressure
757	effects on surface Mediterranean prokaryotes and biogenic silica dissolution during a
758	diatom sinking experiment. Aquatic Microbial Ecology 43: 267–276.
759	doi:10.3354/ame043267
760	Thiele, S., B. M. Fuchs, R. Amann, and M. H. Iversen. 2015. Colonization in the Photic Zone and
761	Subsequent Changes during Sinking Determine Bacterial Community Composition in
762	Marine Snow K.E. Wommack [ed.]. Applied and Environmental Microbiology 81: 1463–1471.
763	doi:10.1128/AEM.02570-14
764	Vernette, C. and others. 2022. The Ocean Gene Atlas v2.0: online exploration of the biogeography
765	and phylogeny of plankton genes. Nucleic Acids Research 50: W516–W526.
766	doi:10.1093/nar/gkac420
767	Villalba, L. A., R. Karnatak, HP. Grossart, and S. Wollrab. 2022. Flexible habitat choice of pelagic
768	bacteria increases system stability and energy flow through the microbial loop. Limnology
769	and Oceanography <b>67</b> : 1402–1415. doi:10.1002/lno.12091
770	Weinbauer, M. G. 2004. Ecology of prokaryotic viruses. FEMS Microbiol Rev 28: 127–181.
771	doi:10.1016/j.femsre.2003.08.001
772	Wilhem, W., and C. A. Suttle. 1999. Viruses and Nutrient Cycles in the Sea. 49: 8.
773	Yayanos, A. A. 1995. Microbliology to 10,500 meters in the deep sea. Annual Review of
774	Microbiologyual Rreview <b>49</b> : 777–805.

//5	Zancker, B., A. Engel, and M. Cunliffe. 2019. Bacterial communities associated with individual
776	transparent exopolymer particles (TEP). Journal of Plankton Research 41: 561–565.
777	doi:10.1093/plankt/fbz022
778	Zhang, C. and others. 2018. Evolving paradigms in biological carbon cycling in the ocean. National
779	Science Review <b>5</b> : 481–499. doi:10.1093/nsr/nwy074
780	Zobell, C. E., and F. H. Johnson. 1949. THE INFLUENCE OF HYDROSTATIC PRESSURE ON THE
781	GROWTH AND VIABILITY OF TERRESTRIAL AND MARINE BACTERIA. Journal of bacteriology
782	<b>57</b> : 179–89.
783	Zobell, C. E., and C. H. Oppenheimer. 1950. Some effects of hydrostatic pressure on the
784	multiplication and morphology of marine bacteria. J Bacteriol <b>60</b> : 771–781.
785	doi:10.1128/jb.60.6.771-781.1950
786	
787	
788	
700	
789	

### **Supplementary materials**

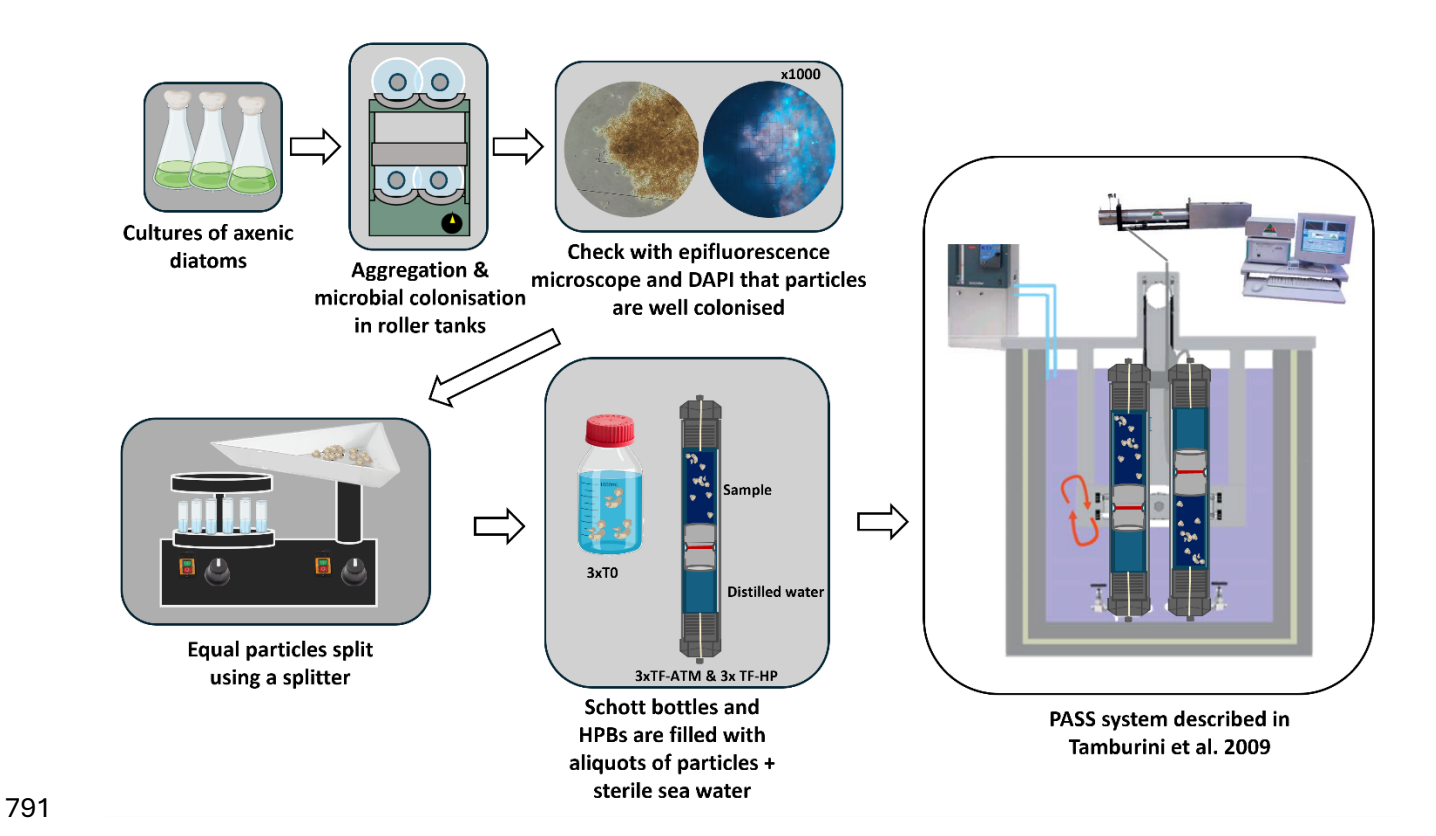


Figure S1: Workflow of the sinking particle simulation experiment using the PASS system.

#### **Oxygen concentrations**

Oxygen concentrations were recorded during the entire incubation using optical oxygen-sensor spots (Presens GmbH R ©, Pst3, detection limit 15 ppb,  $\approx 0.47 \,\mu\text{M}$ ) glued with silicone glue inside the glass Schott bottles or the saphir windows of the HPB lids. A polymeric optical fiber was then held against the spot outside the bottle and was connected to a data logger (OXY-10 mini device for Presens). The procedure and specific adaptation for HPBs is fully described in the method paper by Garel et al. (2019). Oxygen concentration data were then collected every minute during the incubation. All optodes were calibrated manually using a two-point calibration procedure (0 % and 100 % air saturation in MQ water at 25 °C). They were also inter-calibrated individually and intercompared. Effects of hydrostatic pressure, temperature, and salinity were compensated by using algorithms proposed by (Garcia and Gordon 1992; McNeil and D'Asaro 2014).

### Table S2: List of genes known for pressure-induced stress on prokaryotes

Gene Name	Function	KO Number	Reference
ompH	Outer membrane protein for maintaining membrane integrity	K07295	Yano et al. 1998
groEL	Chaperonin, assists in protein folding	K04077	Yano et al. 1998
groES	Co-chaperonin, assists GroEL in protein folding	K04078	Yano et al. 1998
dnaK	Molecular chaperone, helps refold misfolded proteins	K04043	Singh et al. 2004
recA	DNA repair and homologous recombination	K03553	Singh et al. 2004
rpoS	Sigma factor σ^S, regulates stress response genes	K03088	Singh et al. 2004
clpB	Chaperone, involved in protein disaggregation and refolding	K03695	Singh et al. 2004
uspA	Universal stress protein, enhances survival	K03704	Singh et al. 2004
hslVU	ATP-dependent protease complex, degrades misfolded proteins	K01245 (HslV), K01327 (HslU)	Singh et al. 2004
katG	Catalase-peroxidase, detoxifies hydrogen peroxide	K03782	Yayanos et al. 1995
soxRS	Transcriptional regulator, oxidative stress response	K03418 (SoxR), K03419 (SoxS)	Yayanos et al. 1995
ahpC	Alkyl hydroperoxide reductase, reduces organic hydroperoxides	K03386	Singh et al. 2004
trxA	Thioredoxin, maintains cellular redox balance	K03671	Yayanos et al. 1995
grpE	Nucleotide exchange factor, assists DnaK and DnaJ in protein refolding	K03687	Singh et al. 2004
hsp20	Small heat shock protein, prevents protein aggregation	K13993	Yayanos et al. 1995
surA	Periplasmic chaperone, assists in outer membrane protein folding	K03775	Yayanos et al. 1995
hflKC	ATP-dependent protease, involved in membrane protein turnover	K03797 (HflK), K03798 (HflC)	Yayanos et al. 1995
rseA	Negative regulator of sigma E, involved in response to envelope stress	K05873	Alba et al. 2002
degP	Serine protease, involved in protein quality control in the periplasm	K04771	Walsh NP, Alba BM, Bose B, Gross CA.
ftsH	ATP-dependent metalloprotease, involved in protein quality control	K03798	Langklotz et al. 2021
bcsA	Cellulose synthase, involved in biofilm formation	K00694	Ross P, Mayer R, Benziman M. "Cellulose biosynthesis and function".

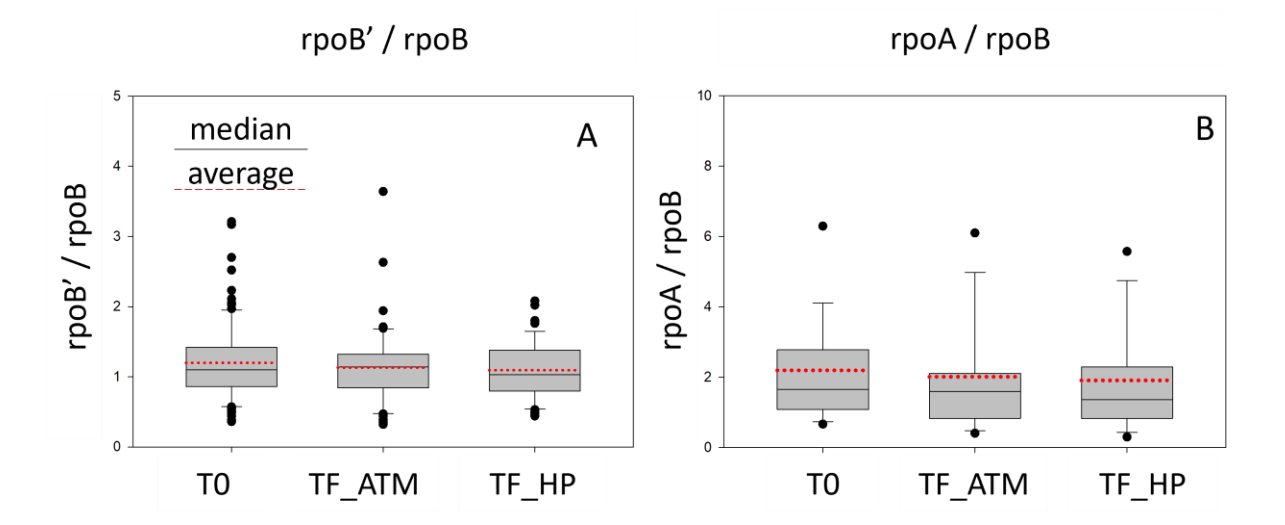
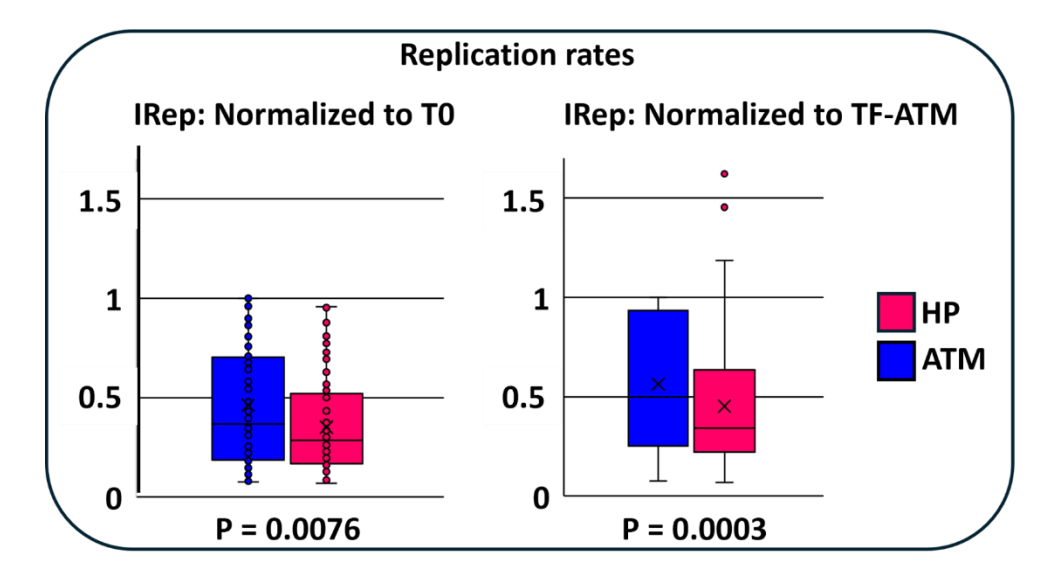


Figure S2: Ratio of housekeeping genes from the DNA-dependent RNA polymerase. Subunit rpoB' (also known rpoC) and rpoB (A) are encoded in the same operon, while subunits rpoA and rpoB (B) are in different genomic locations and under different regulons. The ratios of rpoB' and rpoA to rpoB are constant with differences between conditions being insignificant p=0.78 and p=0.19, respectively (ANOVA on Ranks test). The number of data points per condition are 87, 61 and 63 for T0, TF-ATM and TF-HP, respectively. The constant ratio among conditions suggests that methodological biases have minimal influence on the gene ratios normalized to rpoB, and therefore, statistically significant changes are due to changes in gene expression.



*Figure S3:* Genome replication rates of prokaryotic communities on particles with increasing pressure due to the gravitational sink vs atmospheric pressure (calculated using iRep v1.10 (Brown et al. 2016))

### Table S3: List of genes potentially covering main heterotrophic or chemo-autotrophic pathways

	Gene	Description	KO Number	
	lacZ	beta-galactosidase, involved in lactose utilization	K01190	anic
	galE	UDP-galactose-4-epimerase, involved in galactose metabolism	K01785	or org
	gntK	gluconokinase, involved in gluconate utilization	K00860	olic genes for or, carbon utilization
	fruA	fructokinase, involved in fructose utilization	K00850	olic gr
	xyIA	xylose isomerase, involved in xylose metabolism	K01834	catabolic genes for organic carbon utilization
	xyIB	xylulokinase, involved in xylose metabolism	K00853	
a	fadA	acetyl-CoA acetyltransferase, involved in fatty acid beta-oxidation	K00626	
HETEROTROPHY/ USE OF ORGANIC	fadB	enoyl-CoA hydratase/3-hydroxyacyl-CoA dehydrogenase, involved in fatty acid beta- oxidation	K01025	Genes for fatty acid degradation
JRG	fadE	acyl-CoA dehydrogenase, involved in fatty acid beta-oxidation	K00249	d deg
OF	tnaA	tryptophanase, involved in tryptophan degradation	K01667	atty aci
/ USE	araA	L-arabinose isomerase, involved in arabinose degradation	K01824	ss for f
HY,	araB	L-ribulokinase, involved in arabinose degradation	K00846	Gene
ROF	araD	L-ribulose-5-phosphate 4-epimerase, involved in arabinose degradation	K01784	
ROT	pfkA	phosphofructokinase, a key enzyme in glycolysis	K00850	P
HETE	fbaA	fructose-bisphosphate aldolase, involved in glycolysis and gluconeogenesis	K01623	Genes for glycolysis and gluconeogenesis
	gapA	glyceraldehyde-3-phosphate dehydrogenase, involved in glycolysis	K00134	es for glycolysis gluconeogenesis
	eno	enolase, involved in glycolysis	K01689	es fo
	pykF	pyruvate kinase, involved in glycolysis	K00873	Ger
	gItA	citrate synthase, the first enzyme in the TCA cycle	K01647	cylic
	icdA	isocitrate dehydrogenase, involved in the TCA cycle	K00031	Genes for the tricarboxylic acid (TCA) cycle
	sdhA	succinate dehydrogenase, involved in the TCA cycle	K00239	s for the tricarb acid (TCA) cycle
	fumA	fumarase, involved in the TCA cycle	K01676	s for 1 acid (
	mdh	malate dehydrogenase, involved in the TCA cycle	K00024	Gene

	Gene	Description	KO Number	
INOGRANIC C FIXATION	rbcL	ribulose-1,5-bisphosphate carboxylase/oxygenase large subunit	K01601	Calvin-Benson- Bassham (CBB) Cycle
	rbcS	ribulose-1,5-bisphosphate carboxylase/oxygenase small	K01602	
	prkA	phosphoribulokinase	K00855	288
	acIB	ATP citrate lyase	K15230	Sycle ycle)
	fumA	fumarase	K01676	Reductive TCA Cycle (Reverse TCA Cycle)
	sdhA	succinate dehydrogenase	K00239	ctive erse
	frdA	fumarate reductase	K00244	Redu (Rev
	mcr	methylmalonyl-CoA reductase	K14470	3. Hydroxypropionate Bicycle
	рссВ	propionyl-CoA carboxylase	K01963	3- xyprop Bicycle
	accA	acetyl-CoA carboxylase	K01961	Hydro
	acsB	carbon monoxide dehydrogenase/acetyl-CoA synthase	K14138	Reductive Acetyl- CoA Pathway (Wood-Ljungdahl Pathway)
	fthfs	formate-tetrahydrofolate ligase	K01938	uctive Ac A Pathwa od-Ljungo Pathway)
	mtr	methyltransferase	K00577	Reduct CoA (Wood
	4hbt	4-hydroxybutyryl-CoA dehydratase	K14454	4 Hydroxybu tyrate/3 Hydroxypr
	abfD	4-hydroxybutyrate dehydrogenase	K00333	Hydr tyra Hydr
	sucD	succinyl-CoA synthetase	K01902	Dicarbox ylate/4- Hydroxyb utyrate
	4hbt	4-hydroxybutyryl-CoA dehydratase	K14454	Dic; yla: Hyd uty